Article

Thioxanthone Functionalized NanoTiO₂ Composites as Photocatalyst for Degradation of Organic Dyes

Ya-Xin Li, Dong-Mei Ma,* Rong-Da Zhao, Jun Xiang, and Xingming Zhao*

Cite This: *ACS Omega* 2024, 9, 33081–33089

Read Online

ACCESS | Metrics & More | Article Recommendations

ABSTRACT: Titanium dioxide (TiO_2) photocatalytic technology has the advantages of high catalytic activity, high chemical stability, nontoxicity, and low cost. Therefore, it finds widespread applications in the degradation of organic pollutants in water, antibacterial, environmental purification, and other fields. In this study, we have obtained a photocatalyst by modifying nanoTiO₂ with the photosensitizer thioxanthone. The light-harvesting units of thioxanthone and nanoTiO₂ can work synergistically to capture light energy. As a heterogeneous photocatalytic material, it can efficiently degrade organic dyes such as Rhodamine B, methyl blue and methyl orange. Specifically, the degradation rate of 0.1 mmol/L Rhodamine B can reach 97% after 35 min of irradiation, and methyl blue and methyl orange can also reach 98 and 56%, respectively.

nanoTiO₂P4VPTX
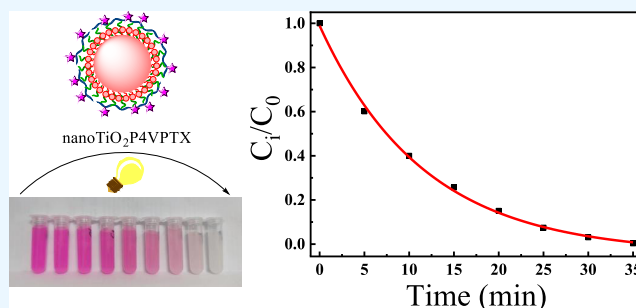
1. INTRODUCTION

Organic dyes are very important chemical raw materials in industrial production, widely used in industries such as textiles, papermaking, and printing. However, they are inevitably released into the environment during production and use, posing a significant threat to water quality, ecological balance, and human health. Therefore, developing efficient and environmentally friendly dye degradation technologies has become an important research focus.[1−5] Among the various dye degradation techniques, photocatalytic degradation has garnered significant attention due to its ease of operation, mild conditions, and absence of secondary pollution. Since the discovery of TiO₂'s photocatalytic properties in 1972, the pursuit of TiO₂ materials with high photocatalytic activity has been a focal point in chemistry, materials science, and environmental science.[6] Although recent years have seen the emergence of various materials, such as transition metal oxides/sulfides/nitrides,[7−11] carbon materials,[12] polyoxometalates,[13,14] and metal−organic frameworks (MOFs),[5,15] that exhibit unique photocatalytic properties, TiO₂ remains a prime choice when considering catalytic activity, production costs, environmental safety, and stability.

The photocatalytic degradation of organic dyes utilizing TiO₂ primarily encompasses the utilization of photoexcited electron−hole pairs, which engage in redox reactions with dye molecules adsorbed onto the surface of the catalyst.[16−20] This process effectively degrades these molecules into innocuous small molecular substances, thereby achieving the desired degradation of organic dyes. However, in practical applications, TiO₂ photocatalysts encounter challenges such as high
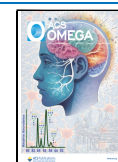
recombination rates of photoexcited electron−hole pairs and a narrow response range to visible light, limiting their effectiveness. To address these issues, researchers have proposed numerous strategies. Doping is one of the effective strategies for enhancing the catalytic efficiency of TiO₂. Introducing metal or nonmetal elements into TiO₂ will change its crystal lattice structure. Appropriate doping may reduce the band gap, allowing higher-wavelength light to be absorbed. Shayegan et al. synthesized Ti^{3+} self-doped TiO₂ microspheres and studied their photocatalytic oxidation performance in a closed cycle system with a gas phase benzene gas mass concentration of 648.9 mg·m⁻³. From the experimental results, Ti^{3+} self-doped TiO₂ samples showed higher photocatalytic activity than undoped TiO₂ samples. Chen et al. successfully modified the surface of 2D-TiO₂ nanosheets with rare-earth single atoms (La, Er) using an impregnation-calcination strategy.[21] Compared to pristine TiO₂, Er_1−TiO₂ and Er^{3+}-TiO₂ exhibited enhanced photogenerated carrier separation capabilities, enabling the production of a higher quantity of reactive oxygen species for the oxidation of volatile organic compounds. Saqlain et al. and Chen et al. used temperature controlled chemical vapor deposition (TR-CVD) to add an

Figure 1. ^{1}H NMR spectrum and structural diagram of P4VPTX.

appropriate amount of Fe to the TiO$_2$ (P25) structure, and demonstrated that the Fe-TiO$_2$ photocatalyst exhibited excellent catalytic degradation of acetaldehyde under visible light at 400−750 nm and significant mineralization ability.[22,23] The composite photocatalysis of TiO$_2$ and semiconductor materials is another effective strategy for removing gaseous pollutants. Guo et al. have effectively combined the biochar adsorption with TiO$_2$ photocatalytic technology to realize the integration of adsorption-photocatalytic degradation of volatile organic compounds.[24] Tobaldi et al. used the green sol gel synthesis method to produce TiO$_2$ and mixed TiO$_2$/graphene materials.[25] The addition of graphene enhances the photocatalytic activity of TiO$_2$. Defect engineering introduces defects into the TiO$_2$ structure through chemical and physical doping. Xie et al. systematically proposed a new method of introducing surface oxygen vacancy defects on TiO$_2$ films using CaH$_2$ as a reducing agent.[26] The obtained TiO$_2$ films can degrade and mineralize benzene using natural light.

Furthermore, forming TiO$_2$ nanocomposites with other materials represents an effective modification method.[27,28] This composite approach combines the strengths of different materials, broadening the spectral response range and enhancing the separation efficiency of photoinduced electron−hole pairs, thereby boosting photocatalytic performance. Zhou et al. conducted surface modification on TiO$_2$ particles with sodium stearate and sodium oleate.[29] After being wet-processed with these agents, TiO$_2$ could turn from hydrophilic to hydrophobic with a controllable degree. Self-assembled monolayers with unique ordered structures and varied anchoring groups have emerged as an excellent interfacial strategy. Chen et al. introduced C-PCBA SAM at the TiO$_2$/perovskite interface to passivate interface defects and improve electron transport.[30]

Thioxanthones (TXs), renowned for their unique photophysical properties, stand out as crucial photosensitizers, distinguished by a remarkable low energy gap separating their singlet and triplet excited states.[31−34] This exceptional characteristic has garnered considerable attention, leading to their exploration in a wide range of applications. TXs have been investigated not just as photocatalysts in various organic reactions,[35,36] but also as effective photoinitiators in processes

such as radical polymerization, photocatalytic organic reactions, and the photocatalytic oxidation of thioethers.[32,35−39] Beyond their application in radical polymerization, TXs have exhibited promising potential in the catalytic photogeneration of N-heterocyclic carbenes[40] and the alkylation of aldehydes,[41] further broadening their photoreactivity scope. To further enhance their absorption capacity and catalytic efficiency, researchers have delved into attaching TX substituents to diphenyl anthracene. This strategic modification has successfully extended the absorption wavelengths of the resulting compounds into the visible light spectrum, enabling their use as visible light photoinitiators.[42] This innovative strategy opens exciting new avenues for the continued development and utilization of TXs in photocatalysis and allied fields, paving the way for future research and applications.

The current study introduces a novel interfacial silane and substitution reaction approach to immobilize TXs onto the surfaces of TiO$_2$ nanoparticles, ultimately yielding TX-functionalized TiO$_2$ nanocomposites. This bottom-up molecular assembly technique at interfaces has garnered significant attention in the creation of innovative materials and diverse multifunctional devices. The synthesis of P4VPTX was followed by its immobilization onto the TiO$_2$ surfaces, leading to the formation of nanoTiO$_2$TX composites. To further investigate their structural and compositional characteristics, various techniques were employed, including thermogravimetric analysis (TG), Fourier transform infrared spectroscopy (FT-IR), UV−vis absorption spectroscopy (UV−vis), and X-ray diffraction (XRD). Photophysical studies revealed intense luminescent emissions centered around 420−434 nm for both TXs and their nanocomposites.

Moreover, these nanoTiO$_2$TX composites exhibited effective photocatalytic activity for the degradation of organic dyes under room temperature conditions. The covalent bonding between the TX monolayers and the nanoparticle surfaces imparted remarkable stability, reusability, and recyclability to the developed photocatalysts, facilitating their facile separation from the reaction system. This study provides valuable insights into the potential applications of TX-functionalized TiO$_2$ nanocomposites in photocatalysis and related fields.
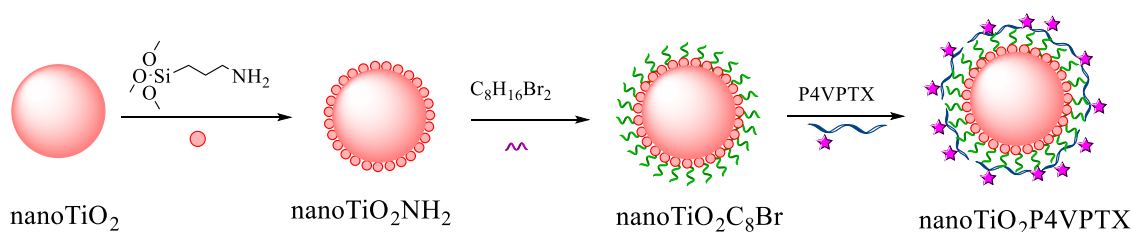
Figure 2. Schematic drawing for the interfacial self-assembly of nanoTiO$_2$P4VPTX composite.

2. MATERIALS AND METHODS

2.1. Materials. The nanoTiO$_2$ was sourced from XFNANO, while 3-aminopropyltrimethoxysilane (APTMS) and thioanisole were procured from J&K Scientific Ltd. (Beijing, China). Additionally, methanol, triethanolamine, ammonia, N,N′-dimethylformamide (DMF), K$_2$CO$_3$, and poly(vinyl alcohol) were purchased from Sinopharm Chemical Reagent Co., Ltd. The 1,8-dibromooctane and 1,4-bis-(bromomethyl)benzene were obtained from Meryer Chemical Technology Co., Ltd. (Shanghai, China). Furthermore, methyl orange, rhodamine B, and methyl blue were acquired from Shanghai Haohong Scientific Co., Ltd. All chemicals were used directly without any further purification.

2.2. Synthesis of nanoTiO$_2$P4VPTX Composites. Under anhydrous and anaerobic conditions, 3-hydroxy-9H-thioxanth-en-9-one (TXOH) was synthesized according to the literature.[38] TXOH (228 mg, 1 mmol), 1,4-bis(benzyloxy)-butane (791 mg, 3 mmol), and anhydrous potassium carbonate (165 mg, 1.2 mmol) were dissolved in anhydrous acetonitrile (30 mL). The mixture was heated to 80 °C and stirred for 15 h under a nitrogen atmosphere. The reaction mixture was cooled to room temperature and extracted with ethyl acetate (30 mL × 3) and water. The combined organic layers were dried over anhydrous magnesium sulfate. After filtration, the organic solvent was removed by reduced pressure distillation. The crude product was purified by rapid column chromatography on silica gel (petroleum ether/ethyl acetate) to afford 3-((4-(bromomethyl)benzyl)oxy)-9H-thioxanthen-9-one TXBenBr as a solid powder (307 mg, 75%). ^{1}H NMR (400 MHz, CDCl$_3$) δ 8.60−8.52 (m, 2 H), 7.60−7.44 (m, 7H), 7.06 (dd, J = 8.8, J = 2.4 Hz, 1 H), 7.06 (d, J = 3.0 Hz, 1 H), 5.13 (s, 2 H), 4.50 (s, 2 H). ^{13}C NMR (400 MHz, CDCl$_3$): δ 178.94, 161.68, 139.43, 138.21, 136.88, 132.68, 131.93, 131.83, 129.67, 129.38, 127.66, 126.16, 125.68, 123.11, 115.52, 109.08, 70.32, 21.19. IR (KBr): λ 3012, 2918, 1628, 1600, 1242 cm^{-1}.

P4VPTX was synthesized by dissolving TXBenBr (200 mg) and poly(4-vinylpyridine) (P4VP, 2 g) separately in chloroform. The TXBenBr solution was then added dropwise to the P4VP solution, and the mixture was heated to 60 °C and stirred for 24 h under a nitrogen atmosphere. The resulting precipitate was collected as P4VPTX. The ^{1}H NMR (400 MHz, CD$_4$O) and structural diagram of P4VPTX are shown in the Figure 1.

To synthesize nanoTiO$_2$P4VPTX composites (Figure 2), we adhered strictly to the procedures described in prior literature sources.[43,44] First, we crafted nanoTiO$_2$NH$_2$ particles by combining TiO$_2$ nanoparticle suspensions with APTMS and maintaining the mixture at 60 °C for a duration of 48 h. Subsequently, the synthesis of nanoTiO$_2$C8Br composites entailed vigorously stirring a blend of nanoTiO$_2$NH$_2$, an excess of 1,8-dibromooctane, and K$_2$CO$_3$ in a DMF solution, maintaining the temperature at 60 °C for another 48 h.

Upon completion of the reaction, the solid nanoTiO$_2$C8Br composite powders were isolated via centrifugation at 4000 rpm. Finally, the suspension nanoTiO$_2$C8Br and P4VPTX in methanol, followed by stirring at room temperature for 24 h at N$_2$ atmosphere, The solid nanoTiO$_2$P4VPTX composite powders were isolated by centrifugation at 4000 rpm, washed thoroughly with dichloroethane until the absence of TX luminescent emissions was confirmed in the filtrate, and finally dried in a vacuum.

2.3. Characterization. ^{1}H and ^{13}C NMR spectra were recorded on a Varian Gemini (400 MHz) spectrometer (Varian Inc., CA), with CDCl$_3$ or CD$_4$O as a solvent and tetramethylsilane as an internal standard. To measure FT-IR, the Nicolet IS50 spectrometer was employed at a temperature of 25 °C. UV−vis spectra were conducted using a Shimadzu UV-1900i system. Thermogravimetric (TG) analysis was performed on an STA 8000 analyzer, heating from room temperature to 800 °C at a rate of 10 °C·min^{-1} under a constant flow of air. The phase composition of the obtained samples was examined by X-ray diffraction (XRD) using a D/max-2500/PC instrument, with Cu Kα radiation (λ = 1.54 Å) and a diffraction angle 2θ ranging from 0 to 90°. The particle size statistics of the composites were detected by the nanoparticle size potentiometer (Zetasizer Nano ZS90). Scanning electron microscopic (SEM) images were captured using a Zeiss-Sigma 500 microscope, operated at an accelerating voltage of 1 kV.

Fluorescence emission spectra, as well as fluorescence quantum efficiency (QE) and time-resolved single photon fluorescence measurements, were recorded using an Edinburgh Instruments FLS-1000 spectrometer, equipped with a microsecond pulsed lamp as the excitation source. Fluorescence lifetimes were estimated from the decay curves of the main transitions, employing the Edinburgh Instruments software package. These lifetimes were calculated based on the equation $\ln(I_t) = \ln(I_0) - (t/\tau)$, where I_0 and I_t represent the fluorescence intensity at time zero and time t, respectively, and τ denotes the experimental lifetime of the excited state of the TXs.

2.4. Photocatalytic. The photocatalytic degradation experiment was conducted within a 50 mL quartz glass photoreactor. The irradiation source for this reactor was a 300W xenon (Xe) lamp, specifically the BL−GHX−Xe−300 model, manufactured by Shanghai Bilon Co. Ltd. in China. To maintain a consistent temperature throughout the experimental process, a circulating water system was employed to regulate the photoreactor's temperature.

The experiment followed a standardized protocol. Initially, 100 mg of the thoroughly dried nanoTiO$_2$P4VPTX composite photocatalyst was uniformly dispersed in a 100 mL aqueous solution containing 0.1 mmol of the organic dye, with methanol serving as the solvent. Subsequently, the mixture

was continuously stirred at room temperature and exposed to ambient air, while being illuminated by the 300W Xe lamp for photocatalytic activation. Prior to irradiation, the mixture was stirred in a darkened environment for 30 min to establish an adsorption equilibrium. Once the equilibrium was reached, the mixture was transferred to the photochemical reactor and irradiated for 40 min, with magnetic stirring maintained throughout. Every 5 min, 5 mL aliquots of the organic dye solution were withdrawn, centrifuged to eliminate catalyst particles, and then analyzed for absorption characteristics using a UV−visible spectrophotometer.

3. RESULTS AND DISCUSSION

3.1. Characterization of Nanocomposites.
Figure 3 displays the TG analysis curves of nanomaterials, spanning
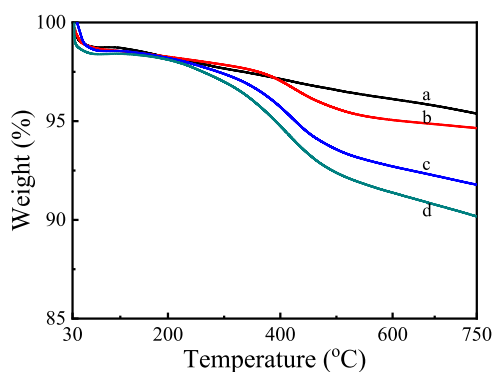
Figure 3. Thermogravimetric curves of (a) nanoTiO$_2$, (b) nanoTiO$_2$NH$_2$, (c) nanoTiO$_2$C8Br and (d) nanoTiO$_2$P4VPTX composites at air atmosphere.

from room temperature to 750 °C in an air atmosphere. The curves consistently exhibit a slight decrease in mass at temperatures below 120 °C, which can be ascribed to the desorption of physically adsorbed water molecules. As for the original nanoTiO$_2$ particles, a gradual weight loss of approximately 3.5% is observed up to 750 °C. And the nanoTiO$_2$NH$_2$ exhibits a weight loss of only 5.4% at 750 °C. This weight loss can be attributed to the thermal decomposition of covalently bound APTMS molecules, as previously reported in the literature.[40,41] Furthermore, upon heating to 750 °C, the TG curves of nanoTiO$_2$C$_8$Br and nanoTiO$_2$P4VPTX composites reveal weight losses of approximately 8.3 and 9.8%, respectively. Notably, the nanoTiO$_2$TX composite exhibits an enhanced weight loss of approximately 1.5% compared to nanoTiO$_2$C8Br, which is attributed to the decomposition of covalently bound P4VPTX substituents.

Figure 4 presents the FT-IR spectra of various composites, including P4VPTX, nanoTiO$_2$, nanoTiO$_2$NH$_2$, nanoTiO$_2$C$_8$Br, and nanoTiO$_2$P4VPTX. All spectra exhibit a broad band centered around 3400 cm^{-1}, which is attributed to the stretching vibration of O−H groups present on the nanoTiO$_2$ particle surfaces, as well as to physically adsorbed water molecules. Notably, the infrared spectrum of the composite displays a distinct peak at approximately 2923 cm^{-1}, arising from the symmetric and asymmetric stretching vibrations of the − CH$_2$− groups. This observation suggests that APTMS is covalently bonded to the nanoTiO$_2$ particle surfaces. Additionally, the composite exhibits a strong absorption band at
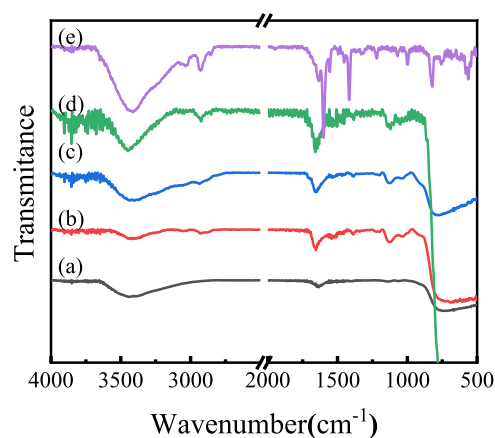
Figure 4. FT-IR spectra of nanoTiO$_2$(a), nanoTiO$_2$NH$_2$(b), nanoTiO$_2$C8Br(c), nanoTiO$_2$P4VPTX(d) composites and P4VPTX-(e).

around 1649 cm^{-1}, attributed to the stretching vibration of the C=O substituent in thioxanthone.

Utilizing dynamic light scattering (DLS) and scanning electron microscopy (SEM), we have performed analysis of the particle size, distribution, and morphological characteristics of the nanocomposite materials. The particle size and distribution of nanoTiO$_2$, nanoTiO$_2$NH$_2$, nanoTiO$_2$C8Br, and nano-TiO$_2$P4VPTX composites in solvents were analyzed using DLS, as depicted in Figure 5. The results reveal that the
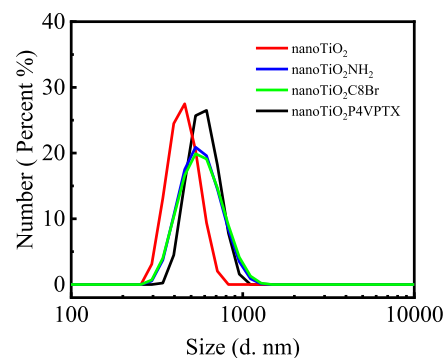

Figure 5. DLS spectra of nanoTiO$_2$, nanoTiO$_2$NH$_2$, nanoTiO$_2$C8Br, and nanoTiO$_2$P4VPTX.

average dynamic particle size of the unmodified nanoTiO$_2$ is approximately 460 nm. After modification with silane compounds and thioxanthone, the average dynamic particle size of the nanoTiO$_2$ material increases. Specifically, the average dynamic particle sizes of nanoTiO$_2$NH$_2$ and nano-TiO$_2$C8Br are approximately 550−600 nm, while the particle diameter of the nanoTiO$_2$P4VPTX composite is about 930 nm. The enlarged dimensions of the modified nanoTiO$_2$ can be attributed to three possible reasons:[45−47] (1) The increased size is affected by the thickness of the organic layer on the surface of the loaded nanoTiO$_2$. (2) Environmental factors, such as solvent molecules surrounding nanoparticles, may affect the movement of particles. (3) Under the influence of the organic layer on the surface of loaded nanoTiO$_2$, interactions between particles lead to the aggregation of nanoparticles, directly resulting in an increase in particle size measured by dynamic light scattering.
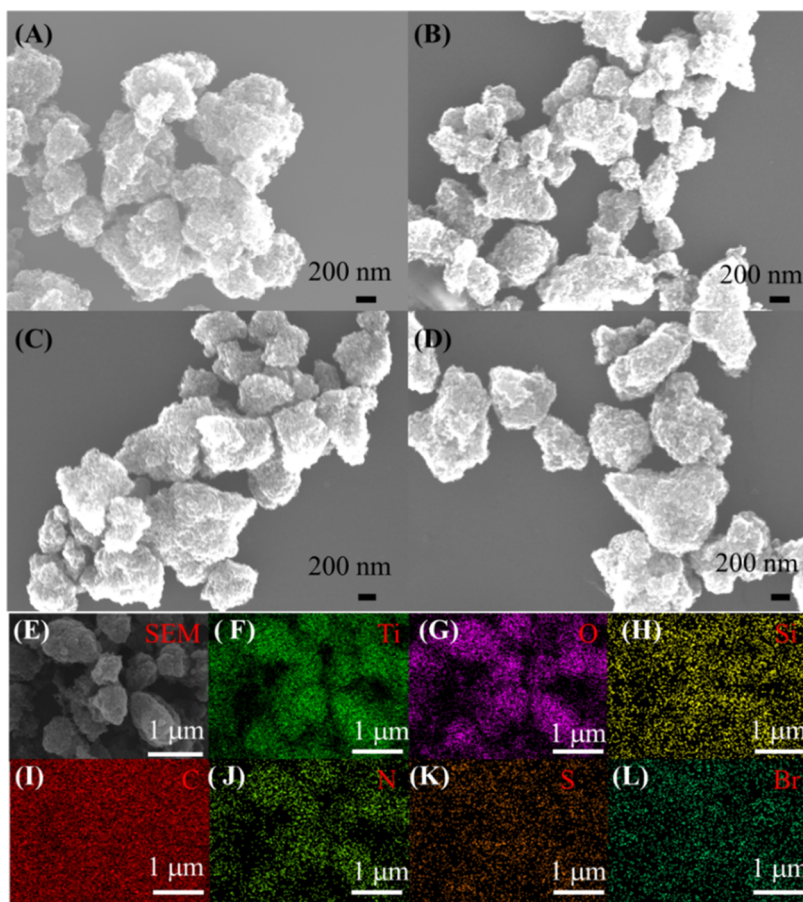
Figure 6. SEM images of (A) nanoTiO$_2$, (B) nanoTiO$_2$NH$_2$, (C) nanoTiO$_2$C8Br, (D) nanoTiO$_2$P4VPTX composite and (E) ∼ (L)EDS surface scanning map of nanoTiO$_2$P4VPTX.

Using SEM, we gained direct visual access to the microscopic images of nanoTiO$_2$ particles, both before and after the integration of P4VPTX. Notably, the particle sizes remained largely consistent, with only subtle variations in aggregation patterns. To provide a vivid representation, Figure 6 shown the SEM images of the nanoTiO$_2$P4VPTX composites. These images confirm that the nanocomposites possess particle sizes approximating 400 nm, aligning with the manufacturer's specifications. As previously reported in the literature,[48] the thickness of the organic layer on the surface of nanocomposites is only approximately 2 nm. Therefore, when comparing SEM images, it is evident that there is no significant change in the morphology of the particles after self-assembly. The only noteworthy observation was an enhanced aggregation tendency among the nanoparticles following surface modification, particularly when modified with TX substituents.

The EDS analysis of the nanoTiO$_2$P4VPTX composite is shown in Figure 6E. It can be seen that the nanoTiO$_2$P4VPTX mainly contains Ti, O, Si, C, N, S and Br elements. This is consistent with the raw materials used to prepare nanoTiO2P4VPTX, indicating the successful preparation of the composite material.

In order to understanding of the composition and structural characteristics of nanoTiO$_2$ and its modified composite materials, XRD analysis was conducted on nanoTiO$_2$, nanoTiO$_2$NH$_2$, nanoTiO$_2$C8Br, and nanoTiO$_2$P4VPTX. As illustrated in Figure 7, all three materials exhibited absorption peaks at specific 2θ angles of 25.2, 37.66, 47.92, 54.92, 62.54,
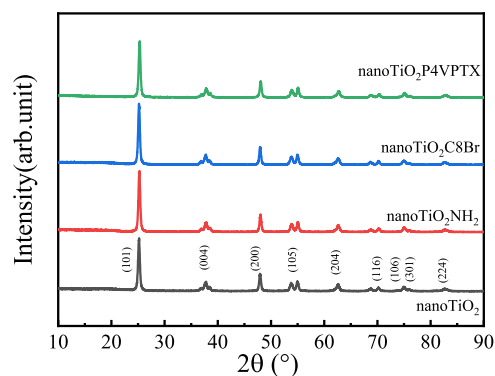
Figure 7. XRD pattens of nanoTiO$_2$, nanoTiO$_2$NH$_2$, nanoTiO$_2$C8Br, and nanoTiO$_2$P4VPTX.

70.16, 74.98, 75.16, and 82.74°. These peaks correspond to the (101), (004), (200), (105), (204), (116), (106), (301), and (224) crystal planes within the nanoTiO$_2$ crystal structure, confirming its tetragonal crystal structure. The grain sizes (D) of TiO$_2$ are calculated using the Scherrer formula

$$D = 0.89\lambda/(\beta \cos \theta) \tag{1}$$

where, β and θ are the full width at half-maximum (FWHM) and diffraction angle of $(101)_{TiO_2}$ peak, λ denotes X-ray wavelength (0.15406 nm) of Cu Kα. The grain sizes of the samples are 21.3, 21.6, 21.5, 21.3, and 22.1 nm, respectively. Notably, the absorption patterns, peak shapes at these 2θ
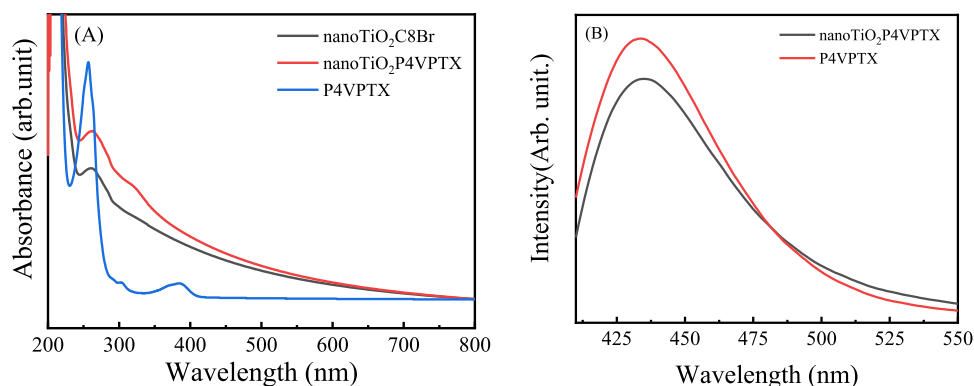
Figure 8. (A) UV−vis absorption spectra nanoTiO$_2$C8Br, nanoTiO$_2$P4VPTX and P4VPTX; (B) luminescent emission spectra and for nanoTiO$_2$P4VPTX and P4VPTX in the methanol solutions.

angles and the grain sizes (*D*) of TiO$_2$ remained largely unchanged across the four materials, indicating that the organic modification of nanoTiO$_2$ did not alter its inherent crystal structure.

3.2. Absorbance and Luminescence. Figure 8A depicts the absorption spectra of nanoTiO$_2$C8Br, nanoTiO$_2$P4VPTX and P4VPTX in methanol. Notably, the absorption spectrum of P4VPTX reveals two prominent absorption bands situated approximately at 258 and 385 nm. These bands can be attributed to the $\pi-\pi^*$ and $n-\pi^*$ electronic transitions inherent to the TX moiety, as referenced in prior studies.[38,49] Upon the formation of nanoTiO$_2$P4VPTX composites, it was observed that these absorption bands persisted in the spectra. Nevertheless, due to the scattering effects caused by the nanoparticles, the peaks were occasionally indistinct.

TXs possess unique properties that render them useful as emitters and hold significant promise for applications in phosphorescent organic light-emitting diodes, as highlighted in previous reports.[45,50,51] The current study delves into the luminescent emission characteristics of P4VPTX and its nanocomposites in methanol solutions. Figure 8B exhibits the luminescent emission spectra of P4VPTX and nano-TiO$_2$P4VPTX in methanol solutions. For P4VPTX and nanoTiO$_2$TX, the excited wavelength was set at 286 nm, a broad emission band was observed for TX, peaking approximately at 434 nm. This emission is attributed to the $\pi-\pi^*$ electron transfer from the excited TX molecules, as reported in prior studies.[43] Interestingly, the emission bands of the nanoTiO$_2$TX composites centered around 435 nm, closely aligning with the emission peak of P4VPTX. The QE of the nanoTiO$_2$P4VPTX composites was 0.028, and the emission lifetimes was 1.35 ns, which accorded well with that reported in the literature.[43]

3.3. Photocatalytic. Industrial wastewater often comprises considerable concentrations of organic and inorganic dyes. This investigation focused on the photocatalytic behavior of nanoTiO$_2$P4VPTX by utilizing organic dyes, namely methyl blue, methyl orange, and rhodamine B, in photodegradation experiments. Initially, a 100 mg nanoTiO$_2$P4VPTX was mixed with 100 mL of an aqueous solution containing the organic dye at 0.1 mmol/L. This mixture was stirred vigorously for 30 min in a darkened environment to establish adsorption equilibrium. In this process, we found that there was a slight change in the concentration of the dye during the adsorption process under dark conditions, as shown in Figure 9. Subsequently, the mixture was transferred to the photochemical reactor, which
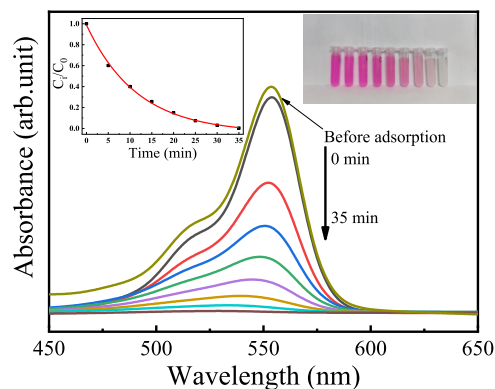

Figure 9. Absorption spectra of rhodamine B aqueous solution containing 100 mg nanoTiO$_2$P4VPTX composites under radiation at the initial 35 min (top to down, before adsorption, 0, 5, 10, 15, 20, 25, 30, and 35 min). (Inserted) A plot of C_i/C_0 to the reaction time.

was maintained at ambient temperature, and irradiated for 35 min under magnetic stirring. Every 5 min, 5 mL aliquots of the organic dye solution of the organic dye solution were extracted and centrifuged using a centrifuge. Finally, an ultraviolet−visible spectrophotometer was employed to analyze the solution, determining its absorption characteristics.

Figure 9 illustrates the effectiveness of the nano-TiO$_2$P4VPTX composite material in degrading rhodamine B under visible light irradiation. As evident from the figure, the absorption peak of the solution near 550 nm gradually diminishes as the irradiation time increases, indicating the gradual degradation of the organic dye in the solution due to light exposure. Additionally, the figure depicts the color change of the organic dye throughout the photocatalytic process. As the irradiation time progresses, the color of the solution gradually transforms from dark to light, ultimately nearing a colorless state.

As the photodegradation products have almost no absorption peak at 550 nm, we estimated the rate of photocatalytic degradation by analyzing the absorption peak intensity at this wavelength, which corresponds to the concentration of Rhodamine B. The included figure illustrates the relationship between the normalized concentration (C_i/C_0) and the irradiation time. Here, C_0 represents the initial concentration of Rhodamine B after achieving adsorption−desorption equilibrium, while C_i denotes its concentration at a specific reaction time, i. Notably, as shown in Figure 10A the newly developed nanocomposites demonstrate the stability
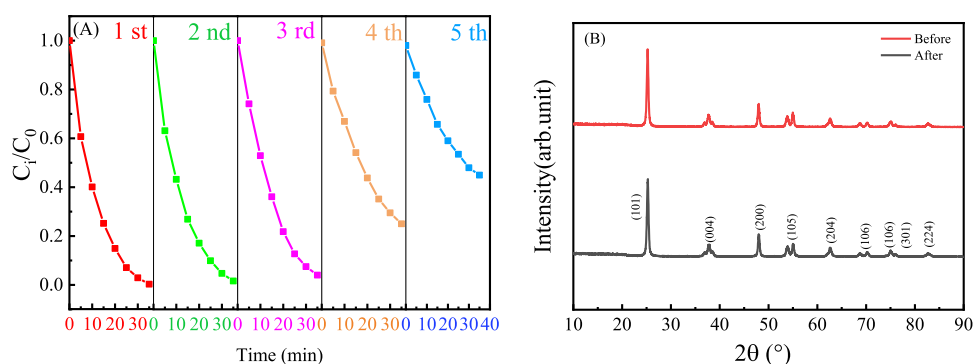
Figure 10. (A) A plot of catalytic efficiency and selectivity to the recycle numbers of the nanoTiO$_2$P4VPTX composites, (B) The XRD patterns of nanoTiO$_2$P4VPTX before and after photocatalytic degradation of rhodamine B.
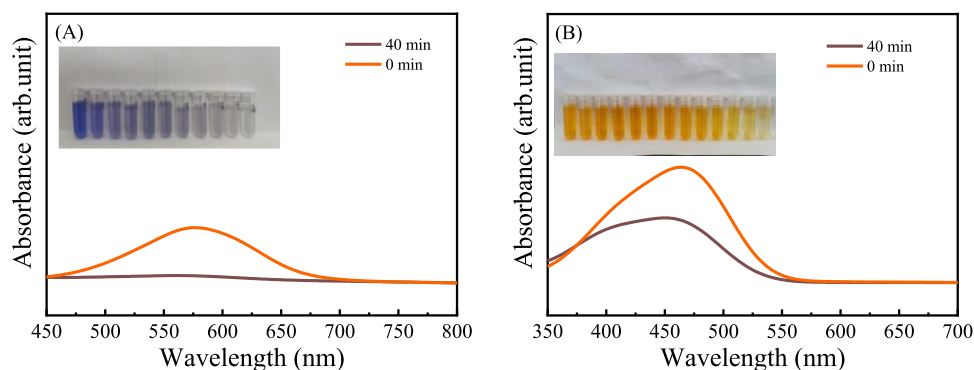

Figure 11. Absorption spectra of methyl blue (A) and methyl orange(B) aqueous solution containing 100 mg nanoTiO$_2$P4VPTX composites under radiation.

and reusability. Although the developed nanocomposites initially exhibited considerable stability and reusability, a decrease in degradation efficiency was observed when they were reused for the fourth time. After repeated use for five times, their degradation efficiency significantly decreased. Potential factors contributing to this observation include: (1) The adsorption of degradation products onto the composite material, which results in the occlusion of active sites and consequently a reduction in the activity of the composite material. (2) Some of the organic active substance TX on the surface of composite materials decomposes under light radiation conditions, leading to a decrease in the catalytic performance of the material.[52] The catalyst nanoTiO$_2$P4VPTX was recovered after undergoing photocatalytic degradation and was subsequently subjected to XRD analysis (Figure 10B). The results demonstrated that the crystal structure of nano-TiO$_2$P4VPTX remained unchanged, compared to its state prior to photocatalytic degradation. This observation conclusively demonstrates the stability of the catalyst, indicating its potential for reliable and sustained performance in photocatalytic applications.

Using organic dyes such as methyl blue and methyl orange, photocatalytic degradation experiments were conducted again using the nanoTiO$_2$P4VPTX composite material. The results are shown in Figure 11. After adding the catalyst to these two organic dyes, the organic dyes were degraded similarly as light exposure progressed, with the color changing from dark to light. As the light exposure time increased, the degradation effect of methyl blue became more pronounced. When the light exposure time reached 40 min, the degradation rate of methyl blue reached 98%; while the degradation rate of methyl

orange reached 56%. These results further demonstrate the potential of our nanoTiO$_2$P4VPTX composite photocatalyst in treating organic pollutants in water.

4. CONCLUSIONS

We demonstrated the interfacial self-assembly of photoactive P4VPTX monolayers onto the surfaces of nanoTiO$_2$, giving rise to TX-functionalized nanocomposites. These nano-composites not only show promise as blue light emitters but also emerge as highly efficient heterogeneous photocatalysts for the degradation of organic dyes under ambient conditions, without the need for high temperatures. The photocatalytic oxidation reaction exhibited remarkable catalytic efficiency. Additionally, as heterogeneous photocatalysts, these nano-composites offer distinct advantages, including ease of separation from the reaction system, outstanding reusability, and recyclability. These benefits stem from the covalent anchoring of the P4VPTX monolayer onto the nanoTiO$_2$ surfaces, ensuring stability and durability in catalytic applications.

■ AUTHOR INFORMATION

Corresponding Authors

Dong-Mei Ma − *School of Materials Science and Engineering, Liaoning University of Technology, Jinzhou 121001, P. R. China;* ⊙ orcid.org/0000-0001-9156-0836; Email: dmma@lnut.edu.cn

Xingming Zhao − *School of Materials Science and Engineering, Liaoning University of Technology, Jinzhou 121001, P. R. China;* Phone: +86-416-4198687; Email: clzxm@lnut.edu.cn

Authors

Ya-Xin Li − *School of Materials Science and Engineering, Liaoning University of Technology, Jinzhou 121001, P. R. China*

Rong-Da Zhao − *School of Materials Science and Engineering, Liaoning University of Technology, Jinzhou 121001, P. R. China*

Jun Xiang − *School of Materials Science and Engineering, Liaoning University of Technology, Jinzhou 121001, P. R. China*

Complete contact information is available at:
https://pubs.acs.org/10.1021/acsomega.4c04243

Notes

The authors declare no competing financial interest.

■ REFERENCES

(1) Teh, C. M.; Mohamed, A. R. Roles of titanium dioxide and ion-doped titanium dioxide on photocatalytic degradation of organic pollutants (phenolic compounds and dyes) in aqueous solutions: A review. *J. Alloys Compd.* **2011**, *509* (5), 1648−1660.

(2) Ullah, R.; Dutta, J. Photocatalytic degradation of organic dyes with manganese-doped ZnO nanoparticles. *J. Hazard. Mater.* **2008**, *156* (1−3), 194−200.

(3) Khataee, A. R.; Kasiri, M. B. Photocatalytic degradation of organic dyes in the presence of nanostructured titanium dioxide: Influence of the chemical structure of dyes. *J. Mol. Catal. A: Chem.* **2010**, *328* (1−2), 8−26.

(4) Tayade, R. J.; Surolia, P. K.; Kulkarni, R. G.; Jasra, R. V. Photocatalytic degradation of dyes and organic contaminants in water using nanocrystalline anatase and rutile TiO_2. *Sci. Technol. Adv. Mater.* **2007**, *8* (6), 455−462.

(5) Yang, H.; He, X. W.; Wang, F.; Kang, Y.; Zhang, J. Doping copper into ZIF-67 for enhancing gas uptake capacity and visible-light-driven photocatalytic degradation of organic dye. *J. Mater. Chem.* **2012**, *22* (41), 21849−21851.

(6) Fujishima, A.; Honda, K. Electrochemical photolysis of water at a semiconductor electrode. *Nature* **1972**, *238*, 37−38.

(7) Nazim, M.; Khan, A. A. P.; Asiri, A. M.; Kim, J. H. Exploring rapid photocatalytic degradation of organic pollutants with porous cuo nanosheets: synthesis, dye removal, and kinetic studies at room temperature. *ACS Omega* **2021**, *6* (4), 2601−2612.

(8) Su, F.; Li, P. P.; Huang, J. S.; Gu, M. J.; Liu, Z. Y.; Xu, Y. H. Photocatalytic degradation of organic dye and tetracycline by ternary Ag_2O/AgBr-CeO_2 photocatalyst under visible-light irradiation. *Sci. Rep.* **2021**, *11* (1), No. 85.

(9) Caglar, B.; Guner, E. K.; Ersoy, S.; Caglar, S.; Özdemir, A. O.; Özdokur, K. V.; Dogan, B.; Icer, F.; Cirak, C. Bi_2S_3 nanorods decorated on bentonite nanocomposite for enhanced visible-light-driven photocatalytic performance towards degradation of organic dyes. *J. Alloys Compd.* **2021**, *885*, No. 160964.

(10) Geng, A. X.; Zhang, Y. B.; Xu, X. L.; Bi, H. T.; Zhu, J. J. Photocatalytic degradation of organic dyes on Li-doped graphitic carbon nitrides. *J. Mater. Sci.: Mater. Electron.* **2020**, *31* (5), 3869−3875.

(11) Barman, D.; Paul, S.; Ghosh, S.; De, S. K. Cu_3N nanocrystals decorated with au nanoparticles for photocatalytic degradation of organic dyes. *ACS Appl. Nano Mater.* **2019**, *2* (8), 5009−5019.

(12) Kumar, O. P.; Ahmad, M.; Nazir, M. A.; Anum, A.; Jamshaid, M.; Shah, S. S. A.; Rehman, A. Strategic combination of metal-organic frameworks and C_3N_4 for expeditious photocatalytic degradation of dye pollutants. *Environ. Sci. Pollut. Res.* **2022**, *29* (23), 35300−35313.

(13) Li, T. H.; Gao, S. Y.; Li, F.; Cao, R. Photocatalytic property of a keggin-type polyoxometalates-containing bilayer system for degradation organic dye model. *J. Colloid Interface Sci.* **2009**, *338* (2), 500−505.

(14) Xu, L. J.; Zhou, W. Z.; Zhang, L. Y.; Li, B.; Zang, H. Y.; Wang, Y. H.; Li, Y. G. Organic-inorganic hybrid assemblies based on Ti-substituted polyoxometalates for photocatalytic dye degradation. *CrystEngComm* **2015**, *17* (19), 3708−3714.

(15) Singh, A.; Singh, A. K.; Liu, J. Q.; Kumar, A. Syntheses, design strategies, and photocatalytic charge dynamics of metal-organic frameworks (MOFs): a catalyzed photo-degradation approach towards organic dyes. *Catal. Sci. Technol.* **2021**, *11* (12), 3946−3989.

(16) Park, H.; Park, Y.; Kim, W.; Choi, W. Surface modification of TiO_2 photocatalyst for environmental applications. *J. Photochem. Photobiol., C* **2013**, *15*, 1−20.

(17) Low, J. X.; Cheng, B.; Yu, J. G. Surface modification and enhanced photocatalytic CO_2 reduction performance of TiO_2: a review. *Appl. Surf. Sci.* **2017**, *392*, 658−686.

(18) He, F.; Meng, A. Y.; Cheng, B.; Ho, W. K.; Yu, J. G. Enhanced photocatalytic H_2-production activity of WO_2/TiO_2 step-scheme heterojunction by graphene modification. *Chin. J. Catal.* **2020**, *41* (1), 9−20.

(19) Razmjou, A.; Mansouri, J.; Chen, V. The effects of mechanical and chemical modification of TiO_2 nanoparticles on the surface chemistry, structure and fouling performance of PES ultrafiltration membranes. *J. Membr. Sci.* **2011**, *378* (1−2), 73−84.

(20) Kumar, S. G.; Rao, K. Comparison of modification strategies towards enhanced charge carrier separation and photocatalytic degradation activity of metal oxide semiconductors (TiO_2, WO_3 and ZnO). *Appl. Surf. Sci.* **2017**, *391*, 124−148.

(21) Chen, J.; Chen, L.; Wang, X.; Sun, J.; Chen, A.; Xie, X. Er single atoms decorated TiO_2 and Er^{3+} ions modified TiO_2 for photocatalytic oxidation of mixed VOCs. *Appl. Surf. Sci.* **2022**, *596*, No. 153655.

(22) Saqlain, S.; Cha, B. J.; Kim, S. Y.; Ahn, T. K.; Park, C.; Oh, J.-M.; Jeong, E. C.; Seo, H. O.; Kim, Y. D. Visible light-responsive Fe-loaded TiO_2 photocatalysts for total oxidation of acetaldehyde: Fundamental studies towards large-scale production and applications. *Appl. Surf. Sci.* **2020**, *505*, No. 144160.

(23) Chen, M.; Wang, H.; Chen, X.; Wang, F.; Qin, X.; Zhang, C.; He, H. High-performance of Cu-TiO_2 for photocatalytic oxidation of formaldehyde under visible light and the mechanism study. *Chem. Eng. J.* **2020**, *390*, No. 124481.

(24) Guo, D.; Feng, D.; Zhang, Y.; Zhang, Z.; Wu, J.; Zhao, Y.; Sun, S. Synergistic mechanism of biochar-nano TiO_2 adsorption-photo-catalytic oxidation of toluene. *Fuel Process. Technol.* **2022**, *229*, No. 107200.

(25) Tobaldi, D. M.; Dvoranova, D.; Lajaunie, L.; Rozman, N.; Figueiredo, B.; Seabra, M. P.; Skapin, A. S.; Calvino, J. J.; Brezova, V.; Labrincha, J. A. Graphene-TiO_2 hybrids for photocatalytic aided removal of VOCs and nitrogen oxides from outdoor environment. *Chem. Eng. J.* **2021**, *405*, No. 126651.

(26) Xie, H.; Li, N.; Chen, X.; Jiang, J.; Zhao, X. Surface oxygen vacancies promoted photodegradation of benzene on TiO_2 film. *Appl. Surf. Sci.* **2020**, *511*, No. 145597.

(27) Zha, K.; Li, L.; Zhang, J.; Tang, S.; Li, X.; Hai, J.; Fan, D.; Li, M.; Liu, Y.; Lu, Z. Investigation the influence of bay substitution with perylene diimide on the photocatalytic performance of perylene−diimide/TiO_2 composites. *J. Photochem. Photobiol., A* **2024**, *451*, No. 115517.

(28) Zhu, E.; Yang, T.; Du, J.; Liu, C.; Ma, C.; Guo, H. Self-assembled A−D−A type indacenodithiophene-based small conjugated molecule/TiO2 for enhancing the photocatalytic activity. *J. Mater. Chem. B* **2023**, *11* (19), 4296−4307.

(29) Zhou, H.; Sun, S. J.; Ding, H. Surface organic modification of TiO_2 powder and relevant characterization. *Adv. Mater. Sci. Eng.* **2017**, *2017*, No. 9562612.

(30) Chen, Z.; Li, Y.; Liu, Z.; Shi, J.; Yu, B.; Tan, S.; Cui, Y.; Tan, C.; Tian, F.; Wu, H.; Luo, Y.; Li, D.; Meng, Q. Reconfiguration toward self-assembled monolayer passivation for high-performance perovskite solar cells. *Adv. Energy Mater.* **2023**, *13* (3), No. 2202799.

(31) Neumann, M. G.; G, Marcelo H.; E, M. V.; Allen, Norman S.; C, T.; P, Carmen.; C, Fernando. Photophysics and photoreactivity of

substituted thioxanthones. *J. Chem. Soc., Faraday Trans.* **1997**, *93*, 1517−1521.

(32) Piñero Santiago, L. E.; Garcia, C.; Lhiaubet-Vallet, V.; Miranda, M. A.; Oyola, R. Solvent dependence of the photophysical properties of 2-chlorothioxanthone, the principal photoproduct of chlorprothixene. *Photochem. Photobiol.* **2011**, *87* (3), 611−617.

(33) Rai-Constapel, V.; Salzmann, S.; Marian, C. M. Isolated and solvated thioxanthone: a photophysical study. *J. Phys. Chem. A* **2011**, *115* (31), 8589−8596.

(34) Burget, D.; Jacques, P. Dramatic solvent effects on thioxanthone fluorescence lifetime. *J. Lumin.* **1992**, *54*, 177−181.

(35) Christmann, J.; Allonas, X.; Ley, C.; Croutxé-Barghorn, C. The role of ketyl radicals in free radical photopolymerization: new experimental and theoretical insights. *Polym. Chem.* **2019**, *10* (9), 1099−1109.

(36) Williams, J. D.; Nakano, M.; Gérardy, R.; Rincón, J. A.; de Frutos, Ó.; Mateos, C.; Monbaliu, J.-C. M.; Kappe, C. O. Finding the Perfect Match: A Combined Computational and Experimental Study toward Efficient and Scalable Photosensitized [2 + 2] Cycloadditions in Flow. *Org. Process Res. Dev.* **2019**, *23* (1), 78−87.

(37) Niu, S.; Schneider, R.; Vidal, L.; Hajjar-Garreau, S.; Balan, L. Light-assisted synthesis and functionalization of silver nanoparticles with thiol derivative thioxanthones: new insights into the engineering of metal/chromophore nanoassemblies. *J. Nanopart. Res.* **2014**, *16* (9), No. 2620.

(38) Ma, D.-M.; Ding, A.; Guo, H.; Chen, M.; Qian, D.-J. Luminescent properties of newly synthesized thioxanthone-polypyridyl derivatives and their metal-organic complexes. *J. Lumin.* **2019**, *212*, 5−13.

(39) Neumann, M. G.; Schmitt, C. C.; Goi, B. E. Thioxanthone sensitized photodegradation of poly(alkyl methacrylate) films. *J. Appl. Polym. Sci.* **2010**, *115* (3), 1283−1288.

(40) Trinh, T. K. H.; Morlet-Savary, F.; M-S, F.; Pinaud, Julien.; Lacroix-Desmazes, Patrick.; Reibel, Corine.; Joyeux, Cécile.; Le Nouen, D.; Nouen, Didier. Le.; Métivier, Rémi.; Brosseau, Arnaud.; Héroguez, Valérie. Photoreduction of triplet thioxanthone derivative by azolium tetraphenylborate: a way to photogenerate N-heterocyclic carbenes. *Phys. Chem. Chem. Phys.* **2019**, *21* (31), 17036−17046.

(41) Rigotti, T.; Casado-Sánchez, A.; Cabrera, S.; Pérez-Ruiz, R.; Liras, M.; de la Peña O'Shea, V. A.; Alemán, J. A Bifunctional Photoaminocatalyst for the Alkylation of Aldehydes: Design, Analysis, and Mechanistic Studies. *ACS Catal.* **2018**, *8* (7), 5928−5940.

(42) Balta, D. K.; Temel, G.; Goksu, G.; Ocal, N.; Arsu, N. Thioxanthone−Diphenyl Anthracene: Visible Light Photoinitiator. *Macromolecules* **2012**, *45* (1), 119−125.

(43) Ma, D.-M.; Xian, Y.; Ding, A.; Guo, H.; Qian, D.-J. Interfacial self-assembled thioxathone monolayers on the surfaces of silica nanoparticles as efficient heterogeneous photocatalysts for the selective oxidation of aromatic thioethers under air atmosphere. *Colloids Surf., A* **2021**, *611*, No. 125856.

(44) Xian, Y.; Ma, D.-M.; Liu, J.-H.; Qian, D.-J. Coordination-driven self-assembly of nanoZnO hybrids with tripodal zinc terpyridyl-viologen complex multilayers and their photochromic properties. *Colloids Surf., A* **2021**, *629*, No. 127456.

(45) Kobler, J.; Möller, K.; Bein, T. Colloidal Suspensions of Functionalized Mesoporous Silica Nanoparticles. *ACS Nano* **2008**, *2*, 791−799.

(46) de la Calle, I.; Menta, M.; Klein, M.; Maxit, B.; Séby, F. Towards routine analysis of TiO_2 (nano-)particle size in consumer products: evaluation of potential techniques. *Spectrochim. Acta, Part B* **2018**, *147*, 28−42.

(47) Lin, D.; Drew Story, S.; Walker, S. L.; Huang, Q.; Cai, P. Influence of extracellular polymeric substances on the aggregation kinetics of TiO2 nanoparticles. *Water Res.* **2016**, *104*, 381−388.

(48) Niu, D.; Jiang, Y.; Ji, L.; Ouyang, G.; Liu, M. Self-Assembly through coordination and π-stacking: controlled switching of circularly polarized luminescence. *Angew. Chem., Int. Ed.* **2019**, *58* (18), 5946−5950.

(49) Ma, D.-M.; Wang, J.; Guo, H.; Qian, D.-J. Photophysical and electrochemical properties of newly synthesized thioxathone−viologen binary derivatives and their photo-/electrochromic displays in ionic liquids and polymer gels. *New J. Chem.* **2020**, *44* (9), 3654−3663.

(50) Wang, H.; Meng, L.; Shen, X.; Wei, X.; Zheng, X.; Lv, X.; Yi, Y.; Wang, Y.; Wang, P. Highly efficient orange and red phosphorescent organic light-emitting diodes with low roll-off of efficiency using a novel thermally activated delayed fluorescence material as host. *Adv. Mater.* **2015**, *27* (27), 4041−4047.

(51) Li, Y.; Li, X. L.; Chen, D.; Cai, X.; Xie, G.; He, Z.; Wu, Y. C.; Lien, A.; Cao, Y.; Su, S. J. Design strategy of blue and yellow thermally activated delayed fluorescence emitters and their all-fluorescence white oleds with external quantum efficiency beyond 20%. *Adv. Funct. Mater.* **2016**, *26* (38), 6904−6912.

(52) Yu, H.-Y.; Li, H.-J.; Ma, Y.-Y.; Feng, Y.-X.; Qian, D.-J. Interfacial self-assembly of carbon nitride-based nanocomposites with zinc terpyridyl coordination polymers for photocurrent generation and the photocatalytic degradation of organic dyes. *Colloids Surf., A* **2020**, *596*, No. 124702, DOI: 10.1016/j.colsurfa.2020.124702.